A reliable procedure to obtain environmentally relevant nanoplastics proxies

Florent Blancho, Mélanie Davranche, Francesco-Sirio Fumagalli, Giacomo Ceccone, Julien Gigault

View Article Online
View Journal

Environmental Science Nano

Accepted Manuscript

This article can be cited before page numbers have been issued, to do this please use: F. Blancho, M. Davranche, F. FUMAGALLI, G. Ceccone and J. Gigault, *Environ. Sci.: Nano*, 2021, DOI: 10.1039/D1EN00395J.

ROYAL SOCIETY OF CHEMISTRY

rsc.li/es-nano

View Article Online
DOI: 10.1039/D1EN00395J

Environmental Significance Statement

The lack of harmonization in the analytical methods to characterize nanoplastics or to evaluate their ecotoxicological effect in realistic conditions is due to the lack of nanoplastic models. Environmentally relevant models are urgently needed for addressing this emerging pollution. The present work proposes a protocol to produce an environmentally relevant model for nanoplastics (e-nanoplastic). The e-nanoplastics are produced by beached plastic debris from the North Atlantic gyre and floating debris from the great Pacific garbage patch. A method was developed to remove the associated organic matter (OM), using a combined H_2O_2/UV process. The composition, size, and surface properties of the e-nanoplastics were characterized by Pyrolysis-Gas Chromatography-Mass Spectrometry, dynamic light scattering, electronic microscopy, XPS, BET analysis, and potentiometric titration.

A reliable procedure to obtain environmentally relevant nanoplastic proxies

View Article Online
DOI: 10.1039/D1EN00395J

Florent Blancho[1], Mélanie Davranche[1], Francesco Fumagalli[2], Giacomo Ceccone[2], Julien Gigault[3*]

[1]Laboratoire Géosciences Rennes, UMR6118, 263 Avenue Général Leclerc, 35042 Rennes
[2] European Commission, Joint Research Centre (JRC), Via E. Fermi 2749, 21027, Ispra, VA, Italy
[3]TAKUVIK laboratoy, UMI3376 CNRS/Université Laval, Québec, Canada

E-mail contact: julien gigault@takuvik.ulaval.ca

Abstract

More environmentally relevant nanoplastic models are urgently needed. Models of environmental plastics are used to develop analytical methods to get an accurate picture of how nanoplastics behave in natural systems, and to generate data on nanoplastics' environmental fate and impact on living organisms. Despite the recent progress in developing models to mimic nanoplastics, the models that are available do not yet show enough diversity to represent the wide heterogeneity in the physical and chemical properties of environmental nanoplastics. In this paper, we report on the strategy we developed to obtain environmentally relevant nanoplastics by mechanical abrasion and sonication of weathered plastics collected from the natural environment (on the beach, and floating in the water). An organic matter degradation protocol was devised to eliminate any potential organic residues that were initially present on the collected plastic samples. The final nanoplastic suspension contains an average of 400 mg carbon $L^{-1,}$ allowing the surface properties to be characterized by XPS, BET analysis, and potentiometric titration. The size distribution of nanoplastics ranges from 200 to 500 nm, with a heterogenous shape and composition (polyethylene or polypropylene) similar to the nanoplastics observed in marine, coastline, and soil systems.

Keywords: nanoplastics, protocol, characterization, surface, environmental fate

Introduction

Most plastics are engineered to be mechanically, biologically, and chemically resistant, and therefore they persist forever and are accumulating in the environment[1–4]. The accumulation of mesoplastics (5–25 mm) and microplastics (1–5 mm) in the ocean, resulting from plastic debris degradation, is well documented[5–7]. Plastic debris fragmentation leads to nanoscale particles (nanoplastics) as plastic debris continues to degrade[8–11]. Nanoplastics present specific physical and chemical colloidal properties that micro-scale plastics do not, such as Brownian motion and wavelength interaction[12]. Nanoplastics have only recently been identified in the ocean[13], coastal areas[14], and soil[15], and from degradation experiments of plastics[10,16]. However, there is a lack of knowledge regarding their physicochemical properties, surface reactivity, and ecotoxicological impacts.

Due to their low availability in the environment, nanoplastics cannot be collected sufficiently well to develop standardized characterization methods and ecotoxicology tests in the environment. Since measurement procedures and impact assessments are urgently needed, the main challenge is to find accurate and relevant nanoplastic models. Historically, the ecotoxicology community first used polystyrene latex as a nanoplastic model[17–19]. However, recent findings have questioned the efficacy this type of model[12]. Several alternative models were thus proposed. They were mainly produced by polymerization[20–23], milling[24], and other auxiliary methods, such as the laser-based approach[25]. For nanoplastic impact assessments, some of those models are promising regarding the absence of surfactants[21], their traceability[23], and their heterogeneity, size, and shape, which are similar to those observed under environmental conditions[24]. These current nanoplastic models demonstrated that the nanosize of nanoplastics allows them to interact with microorganisms or cells[20,22]. However, the justification for using these models for investigating nanoplastic reactivity with contaminants is limited. Their surface functionalization was *a priori* chosen[21] as no characterization of nanoplastic surface functional groups is available. Finally, recent studies have demonstrated that the size and shape influence nanoplastic retention in porous media and their stability in aqueous systems[26,27].

All of the methods used similar approaches: a polymer or specific monomer is used to produce nanoplastics that are homogeneous in composition and not naturally oxidized. Recently, Davranche et al. (2019) have opened the door to a new way of relevant nanoplastic preparation from the altered surface of microplastics collected from natural systems[28]. Despite the potential of these nanoplastics from nature, the method was not pushed further, and the resulting nanoplastics were only partially described. Altering the outer layer to produce nanoplastic models seem to be promising since 1) plastics are altered from the outside (surface) to the inside in nature[29]; 2) their alteration occurs under

View Article Online
DOI: 10.1039/D1EN00395J

environmental conditions; and 3) their shape and surface functional groups are expected to be environmentally relevant.

Based on Davranche et al. (2019)[28], the present work proposes a protocol to produce an environmentally relevant model for nanoplastics (e-NPs). Environmental nanoplastics are produced using beached plastic debris (BD) from the North Atlantic gyre and floating debris (FD) from the great Pacific garbage patch. Environmental nanoplastic composition, size, and surface properties were characterized by Py-GCMS, DLS, TEM, XPS, BET analysis, and potentiometric titration. Besides the production of an e-NPs model, a method was developed to remove the associated organic matter (OM), using a combined H_2O_2/UV process. These e-NPs open new possibilities for investigating ecotoxicological effects and the environmental fate of plastics.

Materials and methods

Environmental nanoplastics production and organic matter degradation

Beach plastic debris (BD) was collected on Saint Marie Bay beach (Guadeloupe, France) in September 2018. Only beach plastics that were less than 10 cm in diameter were collected. After sieving with a 1 cm grid, pieces of plastic debris were manually separated from the beach matrix (i.e., sand and algae residues). Floating plastic debris (FD) was collected from the North Pacific Garbage Patch in 2015 by Ocean Clean-Up, a non-profit organization dedicated to plastics debris removal from the water system (riverine and oceans) [30,31].

We used 100 g BD and 300 g FD as initial material. The plastic debris was mixed with deionized water (DI) at a 1:5 BD/DI and 1:2 FD/DI ratio (wt/wt) in a square bottle and stirred at 250 rpm (Step 1, Figure S1). The ratio of plastic debris to water was optimized in order to obtain the higher quantity of carbon in the final solution. After 48 h, the suspension was sonicated for 1 hour (Step 2, Figure S1). Microplastics were then separated from the suspension with a 40 µm cut-off filter (cellulose acetate, VWR) (Step 3, Figure S1). Organic matter from algae residues (i.e., Sargassum Algae) associated with plastic debris was removed from the suspension using 1% H_2O_2/UV for 5 hours. Finally, the e-NPs were collected with a 1.2 µm cut-off filter (Glass fiber, Prat DUMAS) (Step 4, Figure S1). After the OM oxidation, ultrafiltration (Amicon, Merck Millipore) was used to remove the extra H_2O_2 and concentrate the e-NPs using an ultrafiltration membrane of 20 kDa molecular-weight cut-off (PES, Microdyn NADIR) (Step 5, Figure S1).

Preliminary experiments were done to validate the oxidation step on algae solutions. These solutions were obtained from a deionized water extraction filtered at 1.2 µm and further oxidized by H_2O_2 /UV. The test was conducted at a different H_2O_2 concentration (i.e., 1, 3, 11, and 18 % v/v) and both with

and without UV exposition (RMR-600, Rayonet) (see S2, Figure S2). As known to be previously effective, the H_2O_2 oxidation was set to 72 h without UV, and 5 h with UV[32–34]. Both reaction times are explained by the slower reaction time of H_2O_2 without UV, than with UV. Then, a detailed OM oxidation study was performed using an e-NPs suspension. Small micro-plastics (< 1 mm) were retrieved by the 40 µm filter (cellulose acetate, VWR) and called environmental micro-plastics (referred to as e-microplastics from now on). The e-NPs OM and e-MPs OM refer to nanoplastics and microplastics that have not been purified of organic matter.

Particle size, shape, and surface analysis

The hydrodynamic size of the particles is analyzed using Dynamic Light Scattering (DLS) (VASCO-Flex, Cordouan Technologies) (see S3 for supplementary information). The geometric size and shape of nanoparticles were also examined by transmission electronic microscopy (TEM) (JEM 2100 HR, Jeol). Samples were prepared by drying 2.5 µL of solution on a carbon grid (Oxford instruments). TEM was operated at 200-kV acceleration voltage with LaB_6 as an electron source.

The e-NPs were analyzed by X-ray photoelectron spectroscopy (XPS) using an AXIS Ultra-DLD (Kratos Analytical, JRC, ISPRA) at a pressure of less than 8×10^{-9} mbar. The specific surface area of the e-NPs was quantified by the BET (Brunnauer Emmet and Teller) method using a Gemini VII instrument (Micromeritics). The proton-reactive site was determined by potentiometric titration using a Titrano unit controlled by the Tiamo software (Metrohm). All solutions were base-titrated under N_2 flux with an NaOH solution of 0.01 M (Honeywell Fluka) (see S4 for supplementary information).

Characterization of e-NPs composition

Total Organic Carbon (TOC) content in grams of carbon per litre was quantified using a TOC-V Shimadzu analyzer (Sugimura and Suzuki 1988). The precision of the TOC measurements was estimated to be ± 5% using a standard potassium hydrogen phthalate solution (Sigma Aldrich). Fluorescence spectroscopy was performed with an FL6500 system (Perkin Elmer). Pyrolysis (Pyrolyzer PY-3030 Frontier Lab) coupled to Gas Chromatography-Mass Spectrometry (Py-GC-MS) (5977B, Agilent Technologies) was used for plastic identification. Before Py-GC-MS analysis, a known volume of samples was evaporated at 45°C in an 80µL pyrolysis cup (Frontier Lab). Pyrolysis was performed at 600°C, and the gas chromatography temperatures were similar to the literature (Dehaut et al. 2016). Pyrolyzates were separated on a C18 capillary column (DB5, 30m, Agilent Technologies), with helium as the carrier gas. The mass spectra of pyrolyzates were then compared to the NIST/EPA/NIH library (NIST 14) values, and to our own laboratory library values, including specific polymer pyrolyzates' mass spectra (see S5). The quantification of spectrum similarity (SS) was performed using the MSD Chemstation algorithm (Agilent Technologies). The polymer

identification was based on non-interferent pyrolyzates (there were no homolog pyrolyzates from OM). Thus, the procedure used to validate the identification of a polymer pyrolyzate was to have a similar Kovats retention index already found from polymer pyrolysis and an SS for at least one specific pyrolyzate > 0.80. Besides the polymer identification, Py-GC-MS is used to monitor the removal of OM. For this purpose, three OM pyrolyzates were selected after being identified on algae samples with the NIST library (SS>0.80): 2C-Phenol, 2C-2-Cyclopentenone, and Indole (see S6). The 2C-phenol has many OM precursors (i.e., non-specific) among peptides, proteins, and lignins. The 2C-2-cyclopentenone has only one precursor: polysaccharides. Molecules that contain N, such as proteins, can be precursors of indole. Combining these pyrolyzates permits us to follow OM degradation across different components.

Results&Discussion

Water extraction and purification of e-NPs

Plastic debris offers an easily extracted altered layer, as shown in Figure 1A. After water extraction, it showed a polished surface (Figure 1B), as confirmed by TEM observations (Figure 1C and 1D). The resultant suspension of beach plastics is highly turbid, suggesting numerous small particles (see turbidity difference between Figure 1E and 1F). After filtration, the organic carbon (OC) content was 71±4.1 and 759±61 mg L^{-1} for beach plastics and floating plastics, respectively. This organic carbon includes both e-NPs and natural organic matter from algae residues (Figure 1G and 1H).

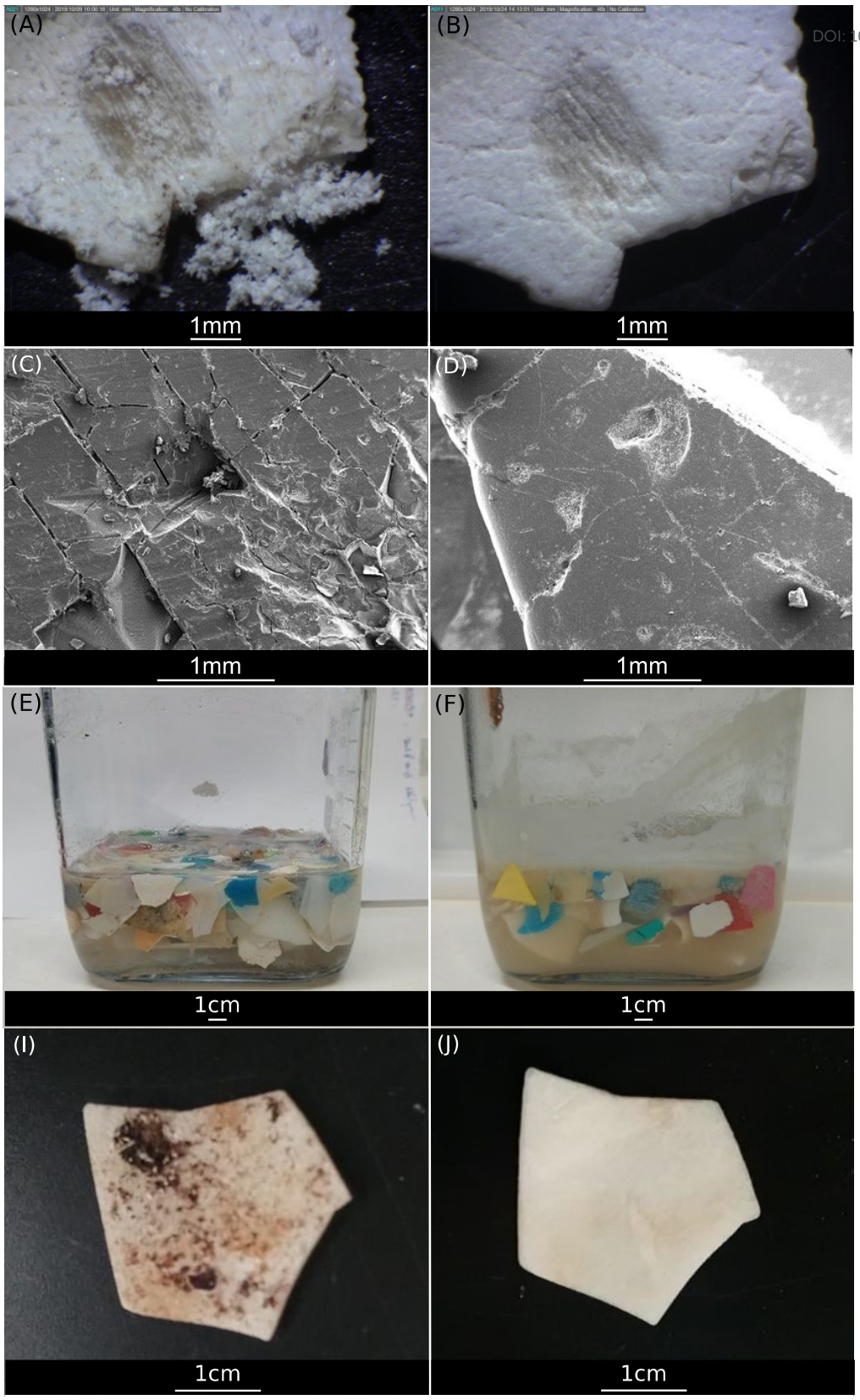

Figure 1: Microplastics and extraction solution before and after applying the extraction protocol on beach plastics. (A), (B) are photography of the same MPs, in detail (A) is the MPs scratched before applying the protocol revealing the weathered layer at its surface and (B), the MPs after using the protocol; (C) and (D) are TEM observations of MPs, before and after using the protocol, respectively; and (E) and (F) showed the extraction solution before and after applying the protocol; (G) and (H) show a microplastic covered by organic materials, before and after using the protocol.

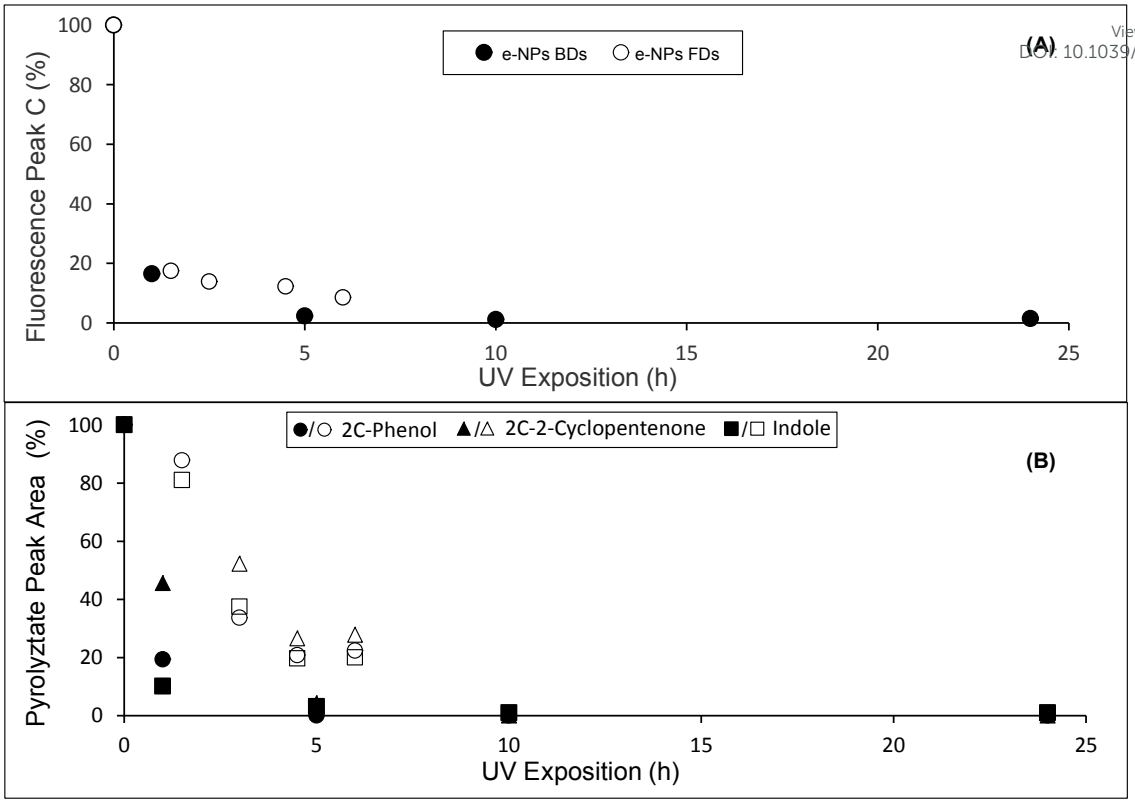

Figure 2:Evolution of organic tracer during OM degradation protocol applied on the e-NPs suspension from beach plastic and floating plastic extraction, filled dot and unfilled dot, respectively; (A) Fluorescence C Peak, obtained by fluorescence spectroscopy; (B) Organic matter.

To remove OM from the plastic suspension, several protocols using basic, acidic, or oxidizing reagents could be used[36–38]. H_2O_2 was shown to be the most efficient for plant matter[38], notably coupled to a catalyzer such as UV light, TiO_2, or ionic Fe(III)/Fe(II) (Vilhunen et al. 2010; Prata et al. 2019). Using H_2O_2 avoids nanoparticle aggregation, compared to basic or acidic reagents. A preliminary investigation demonstrated that photooxidation at 254 nm with 1% H_2O_2 is mandatory to reach more than 95% degradation (see S2). Alnaizy and Akgerman (2000) also demonstrated that temperature inhibits OM degradation from 90% to 30% if the temperature is decreased from 45°C to 20°C. Therefore, the temperature was set to 37°C (regulated in the UV reactor), pH 7 and 1% H_2O_2. This protocol was applied on both suspensions. After OM degradation, the OC content of the e-NPs suspensions reached 5.4±0.1 mg L^{-1} and 331±3.1 mg L^{-1}, respectively, for beach and floating debris. Fluorescence spectroscopy and Pyr-GC-MS were used to validate the OM degradation. 80% of the OM's initial fluorescent C-peak disappears after 5 h of exposure to H_2O_2/UV (Figure 2A)[40,41]. Py-GCMS analysis of the suspension also provided evidence about the disappearance of the OM pyrolyzates (Figure 2B). Note that Figure 2B showed a different efficiency to degrade OM. This may be explained by the order of difference of the initial OC amount. After the concentration step, the concentration reached was 37±1.0 mg L^{-1} and 2038 ±12 mg L^{-1}, for beach and floating plastics,

respectively. Note that the concentration chosen for floating debris was primarily targeted to make the potentiometric titration work.

View Article Online
DOI: 10.1039/D1EN00395J

Environmental nanoplastics polymer identification

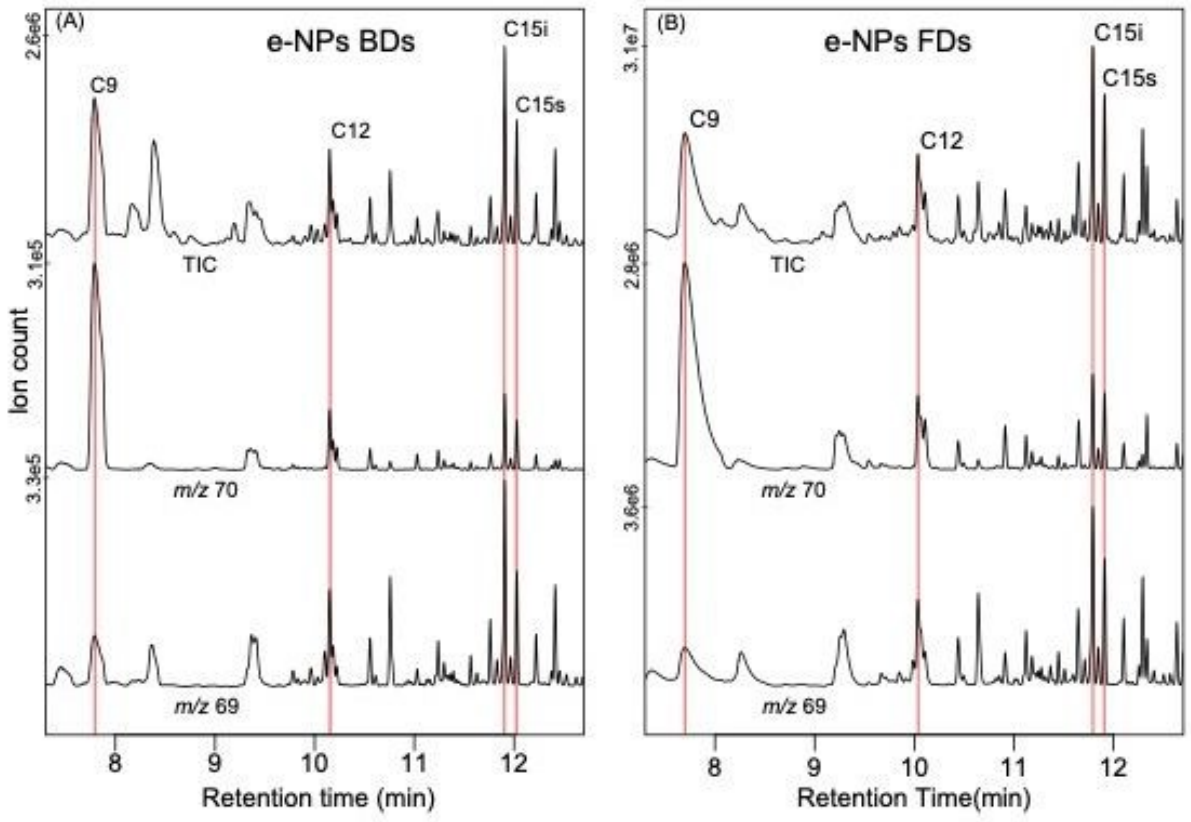

Figure 3: Total Ion, m/z 70 and 69 e-NPs pyrograms from (A) beach debris and (B) floating debris. C9 for 2,4-dimehtyl-1-heptene, C12 for 2, 4, 6-trimethyl-1-nonene (meso form), C15 Isotactic for 2, 4, 6, 8-tetramethyl-1-undecene, C15 Syndiotactic for 2, 4, 6, 8- tetramethyl-1-undecene.

As identified by Dümichen et al. 2017, the pyrolysis of polyethylene produces a class of pyrolyzate with no interferences towards OM pyrolyzates: the alkadienes. These singular markers originate from the scission of long polymer chains, which are not abundant among environmental OM (see SI, Table S3)[42]. For the e-NPs produced from beach debris, none of these PE markers were identified. By contrast, such markers were found for the e-NPs from the floating debris extraction. Three succeeding peaks were identified as alkadienes, as they have similar Kovats retention indices as found in the library, and their spectrum similarities were superior to 0.80 (see S8, Table S4, and *m/z* 81 pyrogram, Figure S3A). Moreover, these markers were followed closely by alkene (*m/z* 97 Figure S3A) as observed during PE pyrolysis (i.e., Figure S3). As a consequence, PE polymer is present in the e-NPs from floating debris.

The identification of polypropylene (PP) succeeds for both suspensions. As already demonstrated for nanoplastics, PP can be identified by the presence of four singular PP pyrolyzates. These 4 PP markers (i.e., C9, C12, C15i, and C15s) were identified in our studies. Indeed, peaks with similar Kovats retention indices showed spectrum similarities > 0.80 (Figure 3, Table S2). Whether for e-NPs suspension of beach or floating debris, PP-identified markers have a dominant height on the total ion pyrogram (TIP). These "fingerprints" suggest that PP is a dominant component of e-NPs.

Size characterization of e-NPs

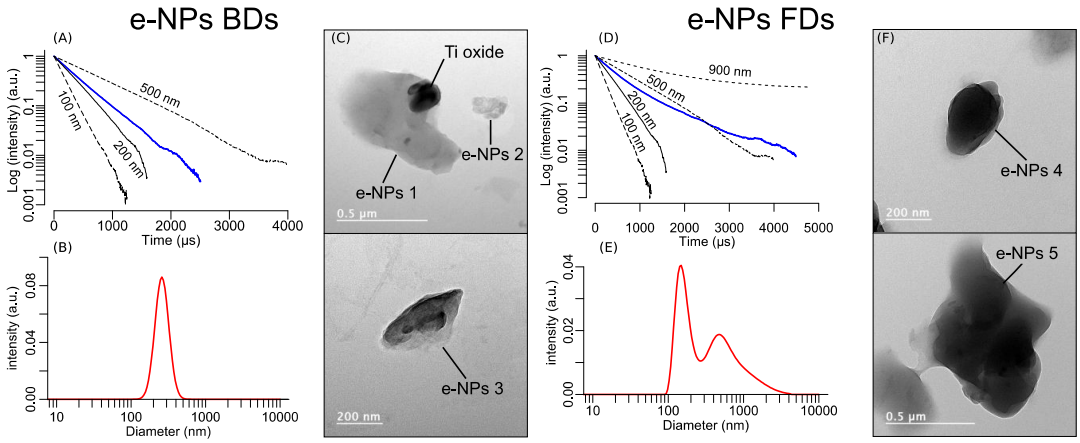

Figure 4: Size characterization of e-NPs from beach and floating debris types. Log-transformed autocorrelation function (blue) and size nominated spherical nanoparticles of polystyrene (black) (A) and (D) for e-NPs from BD and FD, respectively. SBL modelling (red) from the autocorrelation function (B) and I for e-NPs from BD and FD, respectively. TEM images (C) and (F) from BD and FD, respectively. EDX spectrum and atomic composition of e-NPs 1, Ti oxide and the grid are available in SI 9.

Both fractions that were less than 1.2 µm were characterized by DLS and TEM (Figure 4). Figures 4A and 4D displayed the log-transformed time-correlation function of the intensity of light scattered (ACF) obtained by DLS. Compared to spherical size-standardized nanoparticles (polystyrene latex), e-NPs from beach debris present monomodal suspension (i.e., a straight line), with a hydrodynamic diameter ranging from 200 to 500 nm and centered at 250 nm (Sparse Bayesian learning-based modelling). The e-NPs from floating debris are polymodal with an additional colloidal population at a larger size (>500 nm). As shown by the SBL modelling, the first population has a hydrodynamic diameter centered at 150 nm, whereas the second is centered around 500 nm. Note that the SBL predicts particle size >1000 µm; this is modelling bias as the ACF does not cross the ACF from the 900 nm microsphere standard. Transmission electronic microscopic observations displayed anisotropic nanoparticles with sizes <1 µm (Figure 4C and 4F). The carbon intensity of their EDX signal was significantly higher than the grid, suggesting a polymer composition (see S9, Figure S7, and S8). Black cubic particles embedded in the nanoparticle, < 250nm, were also observed. Based on EDX (see S9, Table S6), this cubic particle is composed of Ti and O, suggesting TiO_2. These

View Article Online
DOI: 10.1039/D1EN00395J

nanoparticles are a well-known additive of plastics [43] and were already identified as associated with microplastics [44].

Surface characterization of e-NPs and e-MPs

Overall, the C-C bond is predominant for all samples (> 70%) except for e-NPs OM, where bonds to oxygen are prevalent (~60%) (Figure 5). Dominant C-O bonds for e-NPs OM can be attributed to the algae residue[45,46]. Algae are characterized by considerable water-extractable polysaccharides (> 50%), mainly composed of alginate, laminarin, and mannitol[46–49]. Therefore, the difference in the carbon bond distribution between e-NPs and the e-NPs OM surface is explained by the molecules' release during the e-NPs extraction. More oxidized carbon bonds characterize the e-NPs than for e-microplastics. Moreover, they share similar C=O on their surfaces, whereas O-C=O and C-O bonds are more present on e-NPs. O-C=O (the carboxyl functional group) is interesting as they are known to form complexes with metals[50].

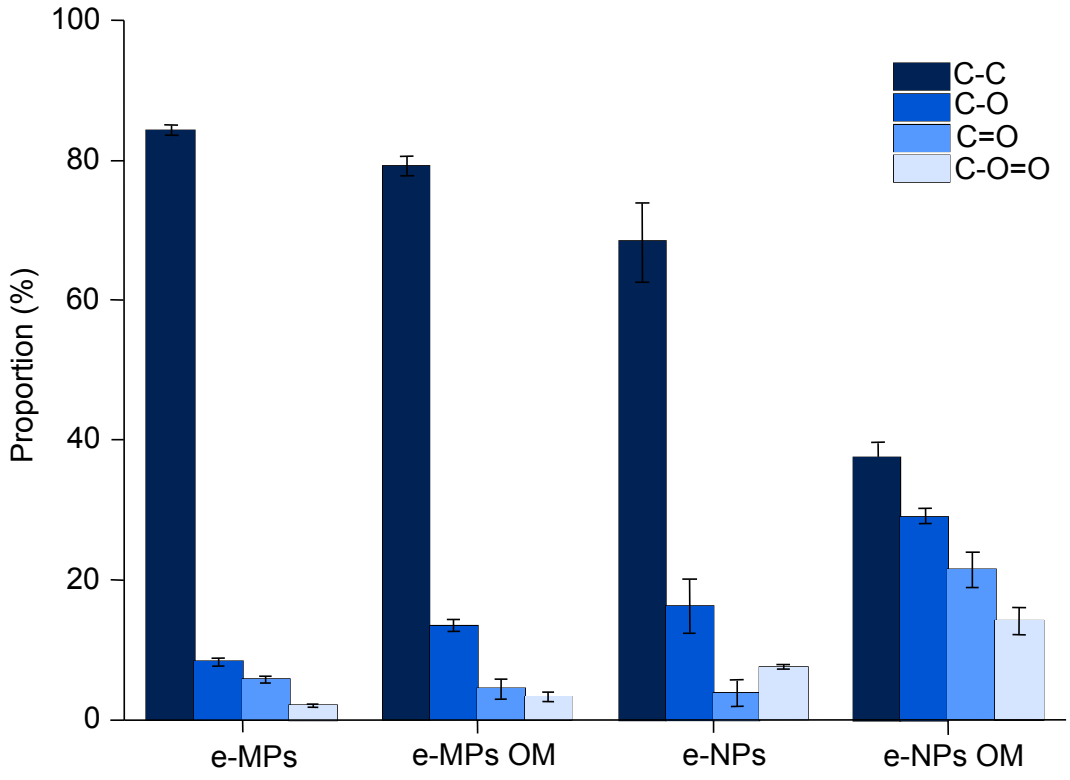

Figure 5: Atomic bonding distribution from C1S. High-resolution spectra from the e-NPs FDs.

During the H_2O_2/UV oxidation, HO• is formed by UV irradiation at 254 nm[51,52]. These radicals can initiate numerous oxidation reactions, which are otherwise limited to photo-reactive impurities (i.e., chromophores). These impurities are included in the polymers during its early production process[53,54]. High concentrations of HO• and HO_2• may affect the termination reaction differently than would

occur in environmental conditions (Chamas et al. 2020). Even if similar functional groups are expected on e-NPs, their density may vary. As shown by XPS, the C bonds at the surface of e-NPs are not drastically different from environmental microplastics and environmental microplastics-OM. This suggests that the H_2O_2/UV oxidation has a limited impact on the e-NPs surface. As H_2O_2 is transparent to λ>300 nm but absorbed the UV radiation at 254 nm, e-NPs were mainly irradiated at λ=315 nm wavelength, as H_2O_2 was in excess (> 0.5% v/v, Figure S11, and Table S8)[51]. Since the backbone bond of PP, PS, PVC, and PE polymers do not absorb at 315 nm[57], the direct UV effect on the e-NPs surface is therefore limited to UVB, as observed in the environment.

Table 1. Physico-chemical properties of e-NPs and environmental phases.

	DLS Analysis			TOC		Potentiometric titration			References
Sample	Model	Number of size populations	Size range (nm)	Conc. (mg L^{-1})	Surface specific (m^2 g^{-1})	H_{surf_tot} (mmol g^{-1})	Site density (sites m^{-2})	ZPC	
e-NPs	Pade-Laplace	2	120-180 and 600-800	200	12.3±2.4	0.225 ± 8.5e-3	11± 0.4	NA	This study
Soil organic matter	-	-	-	-	94-174	14.5	50-92	NA	[58,59]
Ferrihydrite			5	-	350	6	10.32	8.8	[60]
Ferrihydrite	-	-	7	-	650	7.771	7.2	8.0	[61]
Goethite		-	400*40		40	0.11	1.68	-	[62]
Goethite	-	-	500	-	70	0.732	6.3	-	[63]
Gibbsite	-	-	200x10		29.5	0.133	2.71	-	[64]
Montmorillonite	-	-	<2000	-	8.5	0.250	17.41	-	[65,66]
Montmorillonite	-	-	200	-	45.4	0.500	6.63	-	[67,68]
Kaolinite	-	-	< 2000		12.10	0.358	17.8	-	[69]

The surface site on floating e-NPs between pH 4 and 8 was quantified to 0.225 ± 8.5e^{-3} mmol g^{-1}. Among colloids, the e-NPs have proton-reactive sites similar to that of clays, 0.250 mmol g^{-}, but one order of magnitude lower than ferrihydrite and soil OM, 7.77 and 14.5 mmol g^{-1}, respectively (Table 1). The specific surface is determined to equal 12.3 ± 2.4 m² g$^{-1,}$ and the resulting surface site density is calculated to 11.0 ± 0.4 sites m^{-2}. Such density is close to montmorillonite and ferrihydrite, 6.63 and 10.32 sites nm^{-2}, respectively. To summarize, the e-NPs surface has carbon-oxygen functions (C-O, C=O, and O-C=O) estimated at 32 ±6%. Among these oxidized functional groups, 0.225 ± 8.5e-3 mmol g^{-1} were proton-reactive, leading to a surface site density of 13.3±2 sites m^{-2}. Such proton-reactive sites and site density are similar to the reactive colloidal in the environment pictured by clays and ferrihydrite.

Implication for environmental nanoplastics and protocol advantages

Nanoplastic characteristics are poorly understood and studied due to the difficulties of sampling enough material under environmental conditions. The production of environmentally relevant nanoplastic models in large quantities is needed to study their environmental fate, behaviour, and impact. The production of e-NPs with the proposed protocol allows reached concentration of around 400 mg L^{-1}. These concentrations were enough to characterize their composition and surface properties (Table 1). Among the functional group present at the surface of e-NPs, ~10% were identified as carboxylic functional groups (i.e., C-O=O bounds) (Figure 5). These groups explained the proton-reactive sites observed and quantified by potentiometric titration. These results are in accordance with the pH-dependent Pb sorption followed by Davranche et al. 2019. Moreover, as PE and PP carbon skeletons do not include the aromatic cycle, the C-O hydrolyzed bond may be restricted to alcohol functional groups, not known to complex metals [70]. Thus, the sorption capacity of e-NPs may be only due to carboxylic functional groups. However, although one main functional group may drive metal complexation on the e-NPs, these COOH groups may have diverse pKa values due to the presence and proximity of electron-withdrawing groups (carboxylic, acid, ketone, ester, ether, hydroxyl, etc.) on the aliphatic skeleton of PP and PE [70,71].

PP and PE were identified as polymers found in the environmental nanoplastics. This is in accordance with the polymer composition of plastic pieces found in the sea surface and coastal region[9,13,72]. Nevertheless, the PE presence seemed limited as it was not detected for the e-NPs from the beached plastic debris. Moreover, the TIP e-NPs pyrograms show the PP fingerprints with a higher proportion (Figure 3). The higher photooxidation of PP debris certainly explains the observation. Ojeda et al. (2011) observed a higher degradation for PP than for PE after the exact solar light exposition.

Moreover, Fotopoulou et Karapanagioti (2012) observed a significant textural difference between PP and PE plastics[74]. The surface of beached PP was more cracked while PE was more altered. Those

cracks may enhance the removal of the PP altered layer and produce more PP e-NPs than the further application of the present protocol may give an interesting response about the polymer sensitivity to form nanoplastics.

The surface site density of e-NPs was close to that of inorganic colloids, known to be a strong environmental' adsorbent of micropollutants. Therefore, the produced e-NPs are significant sorbents, able to compete with clays and Fe oxyhydroxides. However, about physicochemical properties, two critical differences can be distinguished between these environmental colloids and e-NPs. First, e-NPs do not bear amphoteric hydroxyl sites as observed on Fe oxyhydroxides. These sites can develop negative and positive charges in response to the pH variations[75]. By contrast, e-NPs proton-reactive sites are driven by oxidized carbon functional groups (Figure 5). The e-NPs usually had a charge of zero at acidic pH, and were negatively charged at basic pH values. By contrast, clays and Fe oxyhydroxides always bear negative, and negative or positive charges, respectively[62,68,75]. From a colloidal perspective, these properties explain why e-NPs may be stable or unstable, depending on the environmental conditions. As a consequence, in favourable conditions, nanoplastics may accumulate.

However, the presence of additives or adsorbed elements may affect the net surface charge of the e-NPs, and it is therefore essential to evaluate this surface potential by direct measurement. Also, these surface functionalities are imperative to mimic the metal reactivity of nanoplastics in the environment. Therefore, this first determination of the e-NPs site density could be integrated to produce free soap nanoplastics with realistic site density at their surface [21].

Among the different protocols to produce nanoplastics[21,23–25], using the altered layer from weathered plastics provides numerous advantages, including the realistic presence of random additives, an accurate representative shape and surface morphology, and the presence of oxidized functional groups. Among these groups, a non-negligible part was proton-reactive. The first step of the protocol used in this study is non-degradative, and thus, the extracted e-NPs are the closest model for nanoplastics produced by environmental photooxidation. Another advantage is the possibility to form nanoparticles that are environmentally representative of the plastic made in a specific place under specific conditions. Such properties may be essential for ecotoxicological studies. Moreover, the protocol described here provided quantity of e-NPs to further study their physicochemical properties with consumptive techniques and instruments in this study (XPS, MEB, ATR-FTIR, etc.).

Conclusions

Based on previous work, this study proposed to produce an environmentally relevant nanoplastic model (e-NPs). The e-NPs were obtained by mechanical abrasion and sonication of the altered outer layer found on weathered plastic debris. The efficiency of the process in removing organic matter to purify the e-NPs suspension was assessed by fluorescence spectroscopy and Pyr-GC/M.S. analysis. The yield reached ~80 to 90% depending on the initial concentration of the e-NPs suspension. Purified e-NPs were further characterized in terms of size, shape, composition, and surface properties. The e-NPs produced in this way had a colloidal behaviour in solution, were <1 µm, and had polymorphic shapes as expected for nanoplastics. The e-NPs were composed mainly of polypropylene, but polyethylene was also present. Concerning physicochemical properties, e-NPs were found to contain less than 30% oxidized functional groups (i.e., C=O, C-O, and C-O=O), and a non-negligible proportion were proton-reactive. The density of binding sites on e-NPs was comparable to mineral colloids like clays, which means they are a competing sorbent. The e-NPs are expected to be more stable at high pH values and unstable at low pH, according to the quantity of (de)protonated sites at its surface. Overall, the proposed protocol was successful in producing environmentally relevant nanoplastics. For the first time, we produced a suspension concentration that was sufficient to study nanoplastics' physicochemical properties. These achievements represent substantial progress in nanoplastic model research, and some direct consequences are the further characterizations of the nanoplastics' physicochemical properties, as a better understanding of nanoplastic behaviour and their impacts in the environment. Finally, our protocol offers the opportunity to the scientific community interested to the nanoplastics contamination by using this protocol for specific plastic composition that will be pre-selected.

Acknowledgments

This work was supported by the ANR (Agence Nationale de la Recherche) PRC program through the PEPSEA project (ANR-17-CE34-0008-05). We acknowledge Ludivine Rault for her help during TEM observations performed at THEMIS 476 (ScanMAT, UMS 2001 CNRS - University of Rennes 1).

References

1 D. K. A. Barnes, F. Galgani, R. C. Thompson and M. Barlaz, *Phil. Trans. R. Soc. B*, 2009, **364**, 1985–1998.

2 R. Geyer, J. R. Jambeck and K. L. Law, *Science Advances*, 2017, **3**, e1700782.

3 A. A. Horton, A. Walton, D. J. Spurgeon, E. Lahive and C. Svendsen, *Science of the Total Environment*, 2017, **586**, 127–141.

4 Y. Zhang, S. Kang, S. Allen, D. Allen, T. Gao and M. Sillanpää, *Earth-Science Reviews*, 2020, **203**, 103118.

5 R. C. Thompson, *Science*, 2004, **304**, 838–838.

6 K. L. Law, S. Moret-Ferguson, N. A. Maximenko, G. Proskurowski, E. E. Peacock, J. Hafner and C. M. Reddy, *Science*, 2010, **329**, 1185–1188.

7 A. Cozar, F. Echevarria, J. I. Gonzalez-Gordillo, X. Irigoien, B. Ubeda, S. Hernandez-Leon, A. T. Palma, S. Navarro, J. Garcia-de-Lomas, A. Ruiz, M. L. Fernandez-de-Puelles and C. M. Duarte, *Proceedings of the National Academy of Sciences*, 2014, **111**, 10239–10244.

8 C. Eriksson and H. Burton, *AMBIO: A Journal of the Human Environment*, 2003, **32**, 380–384.

9 J. Reisser, J. Shaw, C. Wilcox, B. D. Hardesty, M. Proietti, M. Thums and C. Pattiaratchi, *PLoS ONE*, 2013, **8**, e80466.

10 J. Gigault, B. Pedrono, B. Maxit and A. Ter Halle, *Environmental Science: Nano*, 2016, **3**, 346–350.

11 J. Gigault, A. ter Halle, M. Baudrimont, P.-Y. Pascal, F. Gauffre, T.-L. Phi, H. El Hadri, B. Grassl and S. Reynaud, *Environmental Pollution*, 2018, **235**, 1030–1034.

12 J. Gigault, H. El Hadri, B. Nguyen, B. Grassl, L. Rowenczyk, N. Tufenkji, S. Feng and M. R. Wiesner, *Nature Nanotechnology*.

13 A. Ter Halle, L. Jeanneau, M. Martignac, E. Jardé, B. Pedrono, L. Brach and J. Gigault, *Environmental Science & Technology*, 2017, **51**, 13689–13697.

14 M. Davranche, C. Lory, C. L. Juge, F. Blancho, A. Dia, B. Grassl, H. El Hadri, P.-Y. Pascal and J. Gigault, *NanoImpact*, 2020, 100262.

15 A. Wahl, C. Le Juge, M. Davranche, H. El Hadri, B. Grassl, S. Reynaud and J. Gigault, *Chemosphere*, 2021, **262**, 127784.

16 S. Lambert and M. Wagner, *Chemosphere*, 2016, **145**, 265–268.

17 P. Bhattacharya, S. Lin, J. P. Turner and P. C. Ke, *The Journal of Physical Chemistry C*, 2010, **114**, 16556–16561.

18 A. Wegner, E. Besseling, E. M. Foekema, P. Kamermans and A. A. Koelmans, *Environmental Toxicology and Chemistry*, 2012, **31**, 2490–2497.

19 E. Besseling, B. Wang, M. Lürling and A. A. Koelmans, *Environmental Science and Technology*, 2014, **48**, 12336–12343.

20 G. Balakrishnan, M. Déniel, T. Nicolai, C. Chassenieux and F. Lagarde, *Environmental Science: Nano*, 2019, **6**, 315–324.

21 L. Pessoni, C. Veclin, H. El Hadri, C. Cugnet, M. Davranche, A.-C. Pierson-Wickmann, J. Gigault, B. Grassl and S. Reynaud, *Environ. Sci.: Nano*, 2019, **6**, 2253–2258.

22 A. G. Rodríguez-Hernández, J. A. Muñoz-Tabares, J. C. Aguilar-Guzmán and R. Vazquez-Duhalt, *Environ. Sci.: Nano*, 2019, **6**, 2031–2036.

23 D. M. Mitrano, A. Beltzung, S. Frehland, M. Schmiedgruber, A. Cingolani and F. Schmidt, *Nature Nanotechnology*, 2019, **14**, 362–368.

24 H. El Hadri, J. Gigault, B. Maxit, B. Grassl and S. Reynaud, *NanoImpact*, 2020, **17**, 100206.

25 D. Magrì, P. Sánchez-Moreno, G. Caputo, F. Gatto, M. Veronesi, G. Bardi, T. Catelani, D. Guarnieri, A. Athanassiou, P. P. Pompa and D. Fragouli, *ACS Nano*, 2018, **12**, 7690–7700.

26 Z. Venel, H. Tabuteau, A. Pradel, P.-Y. Pascal, B. Grassl, H. El Hadri, M. Baudrimont and J. Gigault, *Environ. Sci. Technol.*, 2021, acs.est.0c07545.

27 A. Pradel, H. el Hadri, C. Desmet, J. Ponti, S. Reynaud, B. Grassl and J. Gigault, *Chemosphere*, 2020, **255**, 126912.

28 M. Davranche, C. Veclin, A.-C. Pierson-Wickmann, H. El Hadri, B. Grassl, L. Rowenczyk, A. Dia, A. Ter Halle, F. Blancho, S. Reynaud and J. Gigault, *Environmental Pollution*, 2019, **249**, 940–948.

29 A. ter Halle, L. Ladirat, X. Gendre, D. Goudouneche, C. Pusineri, C. Routaboul, C. Tenailleau, B. Duployer and E. Perez, *Environmental Science & Technology*, 2016, **50**, 5668–5675.

30 C. Lieshout, K. Oeveren, T. Emmerik and E. Postma, *Earth and Space Science*, , DOI:10.1029/2019EA000960.

31 S.-J. Royer and D. D. Deheyn, *mar technol soc j*, 2019, **53**, 13–20.

32 R. Alnaizy and A. Akgerman, *Advances in Environmental Research*, 2000, **4**, 233–244.

33 S. Vilhunen, M. Vilve, M. Vepsäläinen and M. Sillanpää, *Journal of Hazardous Materials*, 2010, **179**, 776–782.

34 M.-T. Nuelle, J. H. Dekiff, D. Remy and E. Fries, *Environmental Pollution*, 2014, **184**, 161–169.

35 Y. Sugimura and Y. Suzuki, *Marine Chemistry*, 1988, **24**, 105–131.

36 A. Dehaut, A.-L. Cassone, L. Frère, L. Hermabessiere, C. Himber, E. Rinnert, G. Rivière, C. Lambert, P. Soudant, A. Huvet, G. Duflos and I. Paul-Pont, *Environmental Pollution*, 2016, **215**, 223–233.

37 S. Kühn, B. van Werven, A. van Oyen, A. Meijboom, E. L. Bravo Rebolledo and J. A. van Franeker, *Marine Pollution Bulletin*, 2017, **115**, 86–90.

38 R. R. Hurley, A. L. Lusher, M. Olsen and L. Nizzetto, *Environmental Science & Technology*, 2018, **52**, 7409–7417.

39 J. C. Prata, J. P. da Costa, A. V. Girão, I. Lopes, A. C. Duarte and T. Rocha-Santos, *Science of The Total Environment*, 2019, **686**, 131–139.

40 P. G. Coble, *Marine Chemistry*, 1996, **51**, 325–346.

41 A. Huguet, L. Vacher, S. Relexans, S. Saubusse, J. M. Froidefond and E. Parlanti, *Organic Geochemistry*, 2009, **40**, 706–719.

42 E. Dümichen, A.-K. Barthel, U. Braun, C. G. Bannick, K. Brand, M. Jekel and R. Senz, *Water Research*, 2015, **85**, 451–457.

43 R. D. Deanin, *Environmental Health Perspectives*, 1975, **11**, 35–39.

44 E. Fries, J. H. Dekiff, J. Willmeyer, M.-T. Nuelle, M. Ebert and D. Remy, *Environmental Science: Processes & Impacts*, 2013, **15**, 1949.

45 A. Dobrinčić, S. Balbino, Z. Zorić, S. Pedisić, D. Bursać Kovačević, I. Elez Garofulić and V. Dragović-Uzelac, *Marine Drugs*, 2020, **18**, 168.

46 P. Yazdani, *Bioresource Technology*, 2015, 7.

47 A. Graiff, W. Ruth, U. Kragl and U. Karsten, *J Appl Phycol*, 2016, **28**, 533–543.

48 R. C. Oliveira, P. Hammer, E. Guibal, J.-M. Taulemesse and O. Garcia, *Chemical Engineering Journal*, 2014, **239**, 381–391.

49 S.-Y. Chee, P.-K. Wong and C.-L. Wong, *J Appl Phycol*, 2011, **23**, 191–196.

50 R. K. Cannan and A. Kibrick, *J. Am. Chem. Soc.*, 1938, **60**, 2314–2320.

51 T. Oppenländer, 2003, 387.

52 L. C. Santos, A. L. Poli, C. C. S. Cavalheiro and M. G. Neumann, *J. Braz. Chem. Soc.*, 2009, **20**, 1467–1472.

53 B. Rånby, *Journal of Analytical and Applied Pyrolysis*, 1989, **15**, 237–247.

54 Jan. F. Rabek, *Polymer Photodegradation*, Springer Netherlands, Dordrecht, 1995.

55 A. Chamas, H. Moon, J. Zheng, Y. Qiu, T. Tabassum, J. H. Jang, M. Abu-Omar, S. L. Scott and S. Suh, *ACS Sustainable Chem. Eng.*, 2020, **8**, 3494–3511.

56 R. Joshi, J. Friedrich and M. Wagner, *Journal of Adhesion Science and Technology*, 2011, **25**, 283–305.

57 B. Rånby and J. F. Rabek, in *Comprehensive Polymer Science and Supplements*, Elsevier, 1989, pp. 253–283.

58 J. W. J. van Schaik, D. B. Kleja and J. P. Gustafsson, *Geochimica et Cosmochimica Acta*, 2010, **74**, 1391–1406.

59 H. de Jonge and M. C. Mittelmeijer-Hazeleger, *Environ. Sci. Technol.*, 1996, **30**, 408–413.

60 M. Villalobos and J. Antelo, 13.

61 T. Hiemstra and W. H. Van Riemsdijk, *Geochimica et Cosmochimica Acta*, 2009, **73**, 4423–4436.

62 L. Lövgren, S. Sjöberg and P. W. Schindler, *Geochimica et Cosmochimica Acta*, 1990, **54**, 1301–1306.

63 M. Villalobos, M. A. Cheney and J. Alcaraz-Cienfuegos, *Journal of Colloid and Interface Science*, 2009, **336**, 412–422.

64 J. Rosenqvist, P. Persson and S. Sjöberg, *Langmuir*, 2002, **18**, 4598–4604.

65 A. Cadene, S. Durand-Vidal, P. Turq and J. Brendle, *Journal of Colloid and Interface Science*, 2005, **285**, 719–730.

66 C. Tournassat, J.-M. Greneche, D. Tisserand and L. Charlet, *Journal of Colloid and Interface Science*, 2004, **273**, 224–233.

67 L. Le Forestier, F. Muller, F. Villieras and M. Pelletier, *Applied Clay Science*, 2010, **48**, 18–25.

68 E. Tombácz and M. Szekeres, *Applied Clay Science*, 2004, **27**, 75–94.

69 I. Jeon and K. Nam, *Sci Rep*, 2019, **9**, 9878.

70 A. E. Martell and R. M. Smith, *Other Organic Ligands*, Springer US, Boston, MA, 1977.

71 J. A. Leenheer, R. L. Wershaw and M. M. Reddy, *Environ. Sci. Technol.*, 1995, **29**, 393–398.

72 K. C. Brignac, M. R. Jung, C. King, S.-J. Royer, L. Blickley, M. R. Lamson, J. T. Potemra and J. M. Lynch, *Environ. Sci. Technol.*, 2019, **53**, 12218–12226.

73 T. Ojeda, A. Freitas, K. Birck, E. Dalmolin, R. Jacques, F. Bento and F. Camargo, *Polymer Degradation and Stability*, 2011, **96**, 703–707.

74 K. N. Fotopoulou and H. K. Karapanagioti, *Marine Environmental Research*, 2012, **81**, 70–77.

75 W. Stumm, Ed., *Aquatic surface chemistry: chemical processes at the particle-water interface*, Wiley, New York, 1987.